Expanded View Figures

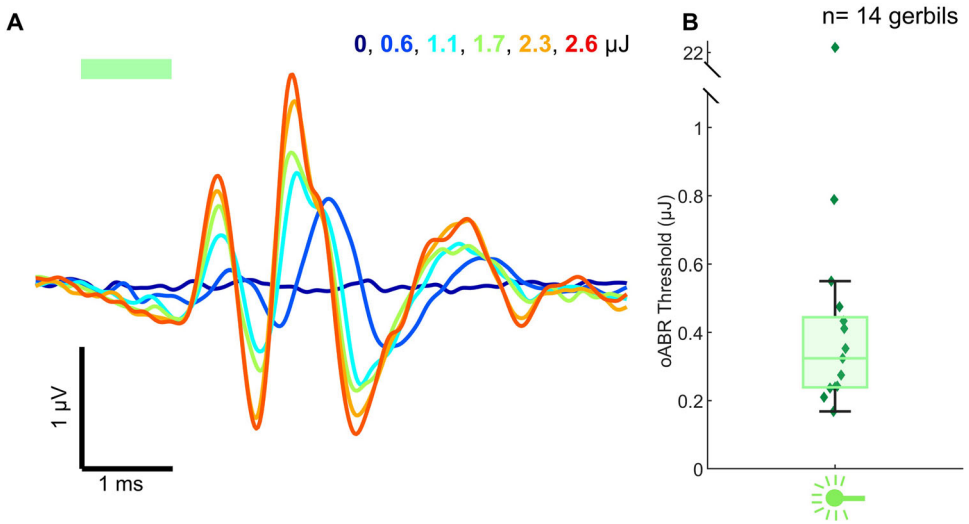


Figure EV1. oABRs evoked by laser stimulation.

(**A**) Representative oABRs evoked by laser stimulation with an optical fiber positioned at the round window of a Mongolian gerbil cochlea. The fiber emitted 522 nm light, delivered as 1 ms pulses at 17 Hz. Colors indicate radiant energy in µJ. (**B**) Radiant-energy thresholds for the occurrence of oABRs under the stimulus conditions shown in (**A**). $n = 14$ gerbils. One gerbil did not show oABR responses. Boxes indicate quartiles and medians; whiskers extend to the most extreme data points within 1.5 × IQR of the box edges; outliers are shown individually.

© The Author(s)

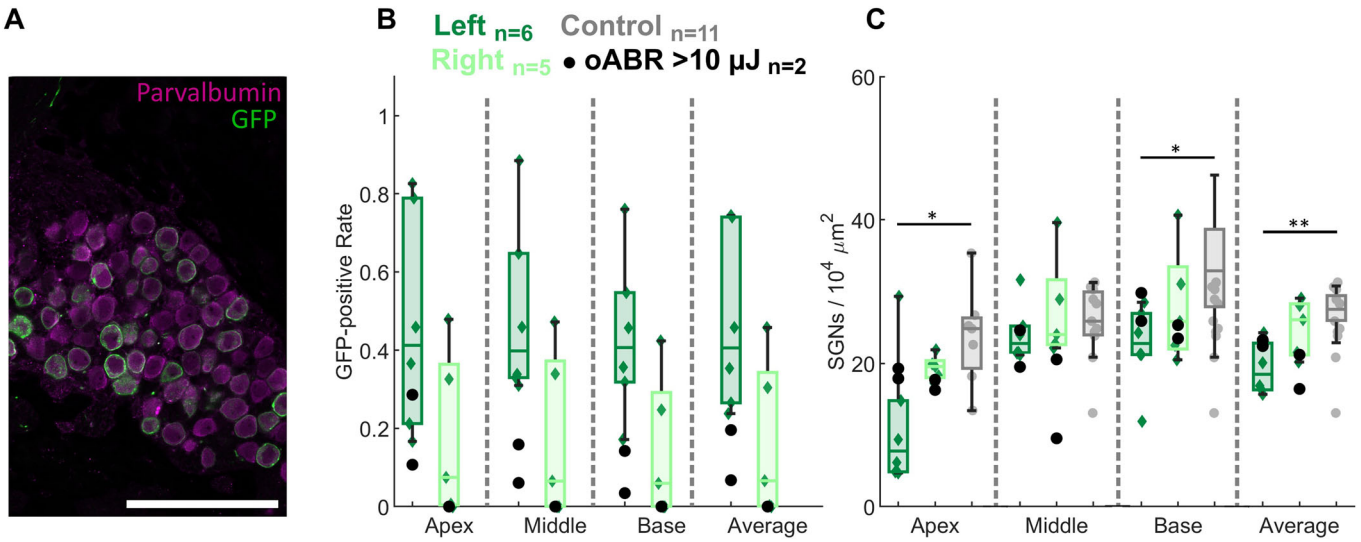


Figure EV2. Immunohistochemical quantification of SGN transduction rate and density.

(**A**) Representative confocal image of immunolabeled SGNs in Rosenthal's canal. SGNs were identified by anti-parvalbumin staining (magenta). Anti-GFP staining was used to label the eYFP tag of ChReef. Scale bar, 100 µm. (**B**) Fraction of GFP-positive SGNs in each cochlear turn as well as averaged across turns of the left, injected cochlea ($n = 7$) and the corresponding right cochlea ($n = 6$). No statistically significant difference was detected using a one-sided Wilcoxon matched-pairs signed-rank test ($p > 0.05$). (**C**) SGN density in each cochlear turn for the groups shown in B, and left, non-injected cochleae from wild-type animals ($n = 11$). Groups were compared using a Kruskal–Wallis test followed by Tukey's multiple-comparisons test (*$p < 0.05$, **$p < 0.01$). Only statistically significant differences are indicated. Exact *p*-values are reported in Dataset EV2. Animals with oABRs detected only at >10 µJ, or with no detectable oABRs, were excluded from statistical testing. Boxes indicate quartiles and medians; whiskers extend to the most extreme data points within 1.5 × IQR of the box edges; outliers are shown individually..

© The Author(s)

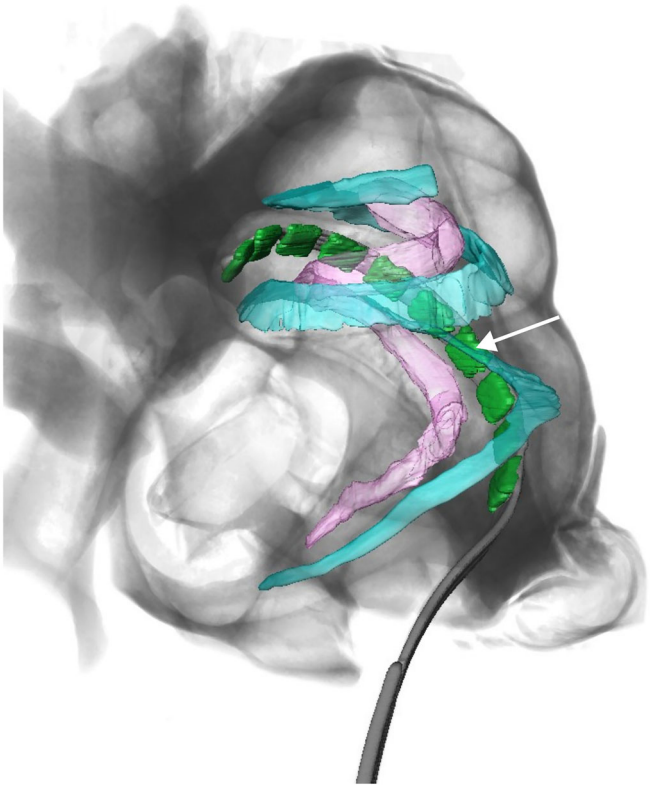


Figure EV3. oCI position relative to the basilar membrane.

X-ray tomography of a gerbil cochlea implanted with an oCI, as in Fig. 1B. The oCI pierced the basilar membrane during implantation. In the position used for stimulation, the implant crossed the basilar membrane near LED 7 (counted from the apex; white arrow). The estimated positions of the basilar membrane (cyan) and Rosenthal's canal (magenta) were segmented and visualized after reconstruction. Individual LEDs measured 220 × 270 µm (width × length along the implant).

© The Author(s)

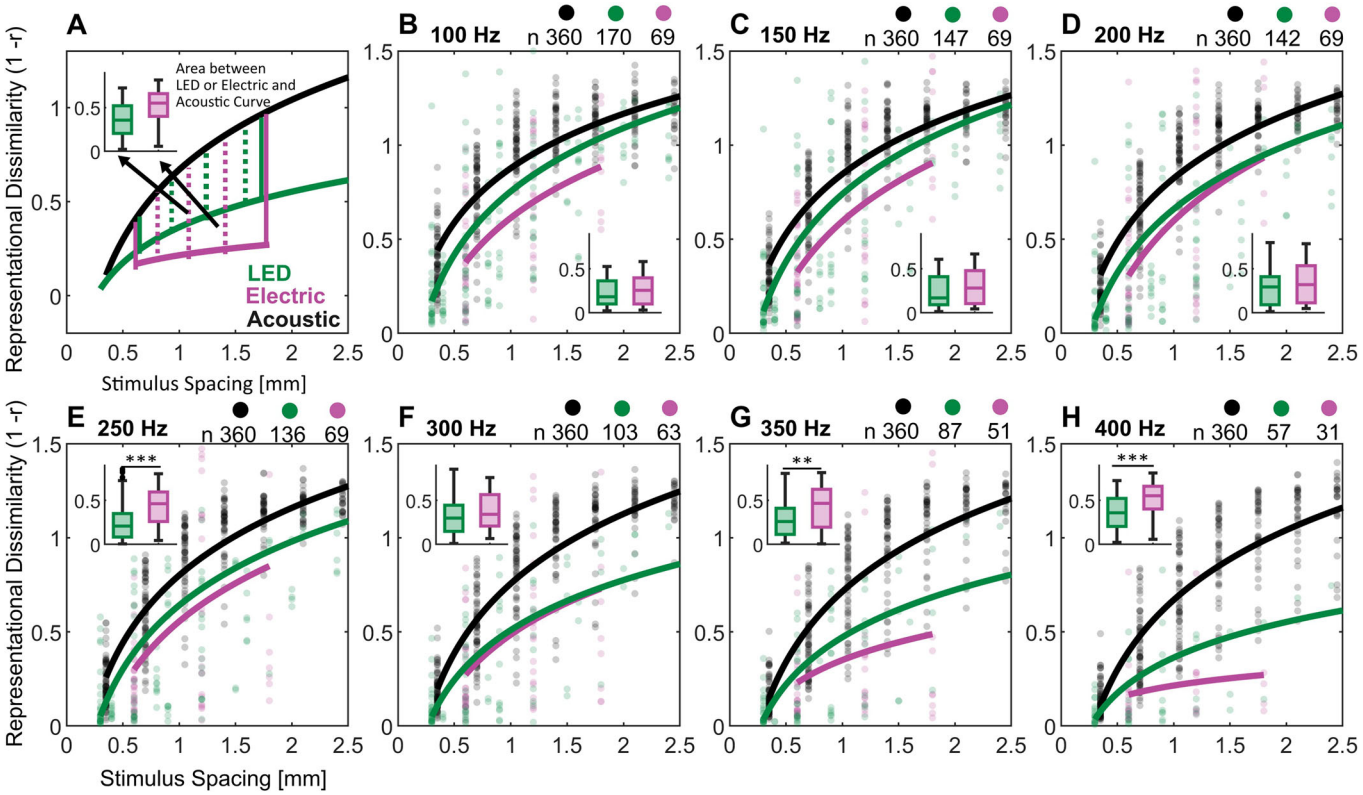


Figure EV4. Representational dissimilarity across firing rates.

(**A–H**) Comparison of representational dissimilarity across stimulus spacings for different stimulation modalities at matched activity levels (columns). Individual data points obtained from $N = 8/8/12$ gerbils for acoustic/optical/electrical, represent representational dissimilarities between stimulus pairs, and are shown in the background. The number of recordings contributing to each modality is indicated above the panels. Modality-specific estimates across animals (solid lines) were obtained at each activity level using linear mixed-effects models (see methods, Dataset EV1). Differences to the acoustic reference were quantified as the areas between the predicted lines for each animal pair (opto-acoustic and electric–acoustic; method illustrated in panel **F**). This analysis was restricted to the activation spacings for which data were available in all modalities (600–1800 µm). The results are shown as boxplot insets. Boxes indicate quartiles and median; whiskers extend to the most extreme data points within 1.5 × IQR of the box edges; outliers are shown individually. The significance of differences between the oCI and eCI condition was assessed using a Mann–Whitney *U*-test. Only significant differences are indicated (*$p < 0.05$, **$p < 0.01$, **$p < 0.001$). Exact *p* values are reported in Dataset EV2.

 © The Author(s)

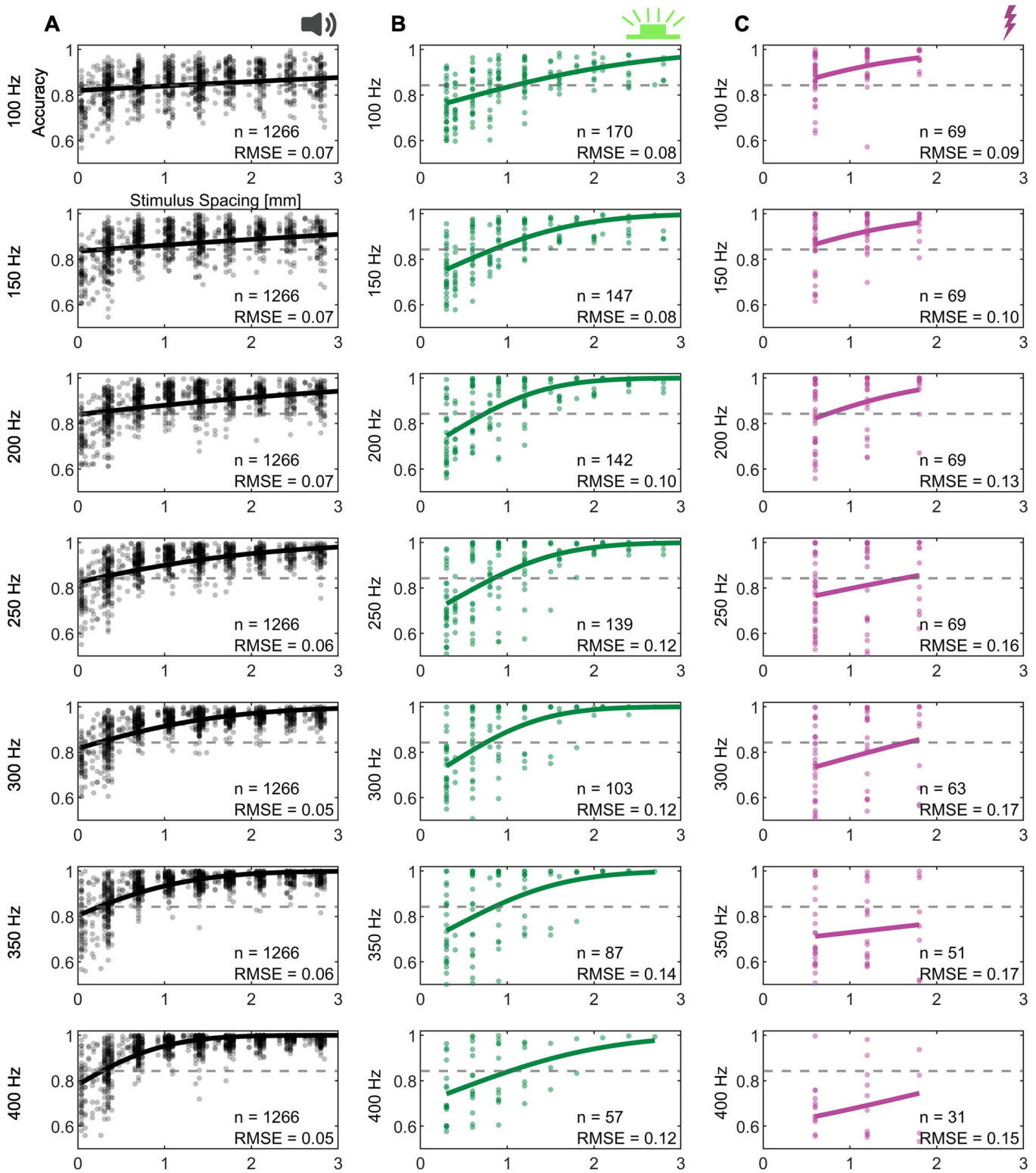


Figure EV5. Neurometric functions at different activity levels for acoustic, electrical and optical stimulation.

(**A–C**) Neurometric functions, as described in Fig. 8B, shown for different activity levels (rows) and stimulus modalities (columns, **A–C**). Background points show decoding accuracy for individual stimulus pairs at each ER, given next to each ordinate. The root mean square error (RMSE) of each fit and the number of data points are indicated in each panel.

© The Author(s)